A&A 450, 1149–1156 (2006)
DOI: 10.1051/0004-6361:20054411

Astronomy & Astrophysics

Time-resolved spectroscopy of the bright sdBV Balloon 090100001⋆,⋆⋆

I. Observations and frequency analysis

J. H. Telting[1] and R. H. Østensen[2]

[1] Nordic Optical Telescope, Apartado 474, 38700 Santa Cruz de La Palma, Spain
e-mail: jht@not.iac.es
[2] Isaac Newton Group of Telescopes, Apartado 321, 38700 Santa Cruz de La Palma, Spain
e-mail: roy@ing.iac.es

Received 25 October 2005 / Accepted 18 January 2006

ABSTRACT

We have obtained 2552 useful low-resolution spectra of the bright sdBV Balloon 090100001, which form the first large time-resolved spectroscopic dataset of this brightest known pulsating subdwarf B star. The data were obtained at the Nordic Optical Telescope during 7 nights in August/September 2004 over a total time base of 38 nights, aiming to derive pulsational characteristics of this star. In this paper we present the observations and the results obtained from frequency analyses. In our data we find clear evidence for 8 independent frequencies, that were all previously reported in photometric monitoring studies, allowing future asteroseismological studies of this star to be constrained by combined photometric and spectroscopic observations of as much as 8 pulsation modes. We do not find conclusive evidence for new frequencies. We present the first determination of the pulsational radial-velocity amplitudes of this star, and find that the radial-velocity amplitude of the main pulsation mode (f_1 = 2.80749 mHz) in Balloon 090100001 is 18.9 km s^{-1}, which is the largest radial-velocity amplitude found in sdB-star pulsations so far. For all spectra, the radial velocities are published electronically.

Key words. stars: subdwarfs – line: profiles – stars: early-type – stars: oscillations – stars: individual: Balloon 090100001

1. Introduction

The subdwarf B (sdB) stars collectively form the relatively cooler population of the hot extreme horizontal branch (EHB) stars. The EHB models imply that they are core helium burning objects with an extremely thin ($M_{\rm env} \leq 0.02\ M_\odot$) inert hydrogen dominated envelope (Heber 1986; Saffer et al. 1994). This configuration prevents them from ascending the asymptotic giant branch, and they must evolve instead towards higher temperatures and surface gravities after their core helium is exhausted. Thus, an sdB star evolves into the hotter sdO population before reaching degeneracy and the associated white-dwarf cooling track (Dorman et al. 1993).

Although the models that describe the future evolution of the sdB stars are generally accepted, their evolution into the sdB stage is controversial. There are several possible scenarios that involve either single star or binary evolution. For the single star scenario, the preferred model requires enhanced mass loss during or after the red giant branch phase (D'Cruz et al. 1996). The problem in this case is how the mass-loss mechanism removes all but a tiny fraction of the hydrogen envelope at *precisely* the same time as the He core has attained the mass (~0.5 $M_\odot$) required for the He flash.

Several possible binary evolution scenarios have been proposed to explain the high number of detected companions to sdB stars. These scenarios all involve close-binary evolution with strong mass transfer in the form of either a common-envelope ejection, stable Roche-lobe overflow or a complete merger of two helium white dwarfs (see e.g. Han et al. 2002, 2003).

Renewed hope that the evolutionary paths leading to the formation of sdB stars can be resolved came after the discoveries of two classes of (non-)radially pulsating sdB stars. These discoveries have opened the possibility of probing the stellar interiors using seismological methods. The two classes have become known as short-period sdB variables (SPsdBVs), or V361 Hya stars (formerly EC 14026 stars) after the prototype, and long-period sdB pulsators (LPsdBVs), or PG 1716 stars.

The short-period pulsators were discovered first (Kilkenny et al. 1997), and a theoretical prediction of the existence of

⋆ Based on observations from the Nordic Optical Telescope.
⋆⋆ Full Table 8 is only available in electronic form at the CDS via anonymous ftp to cdsarc.u-strasbg.fr (130.79.128.5) or via http://cdsweb.u-strasbg.fr/cgi-bin/qcat?J/A+A/450/1149

p-modes due to an opacity bump associated with iron ionisation in subphotospheric layers was made simultaneously (Charpinet 1996, 1997). These stars are characterised by relatively short pulsation periods ranging between ∼1 and 10 min and photometric pulsation amplitudes typically between 0.01 and 0.05 mag. The instability is predicted to occur in the temperature range between about 29 000 K and 37 000 K. However, most stars in this temperature range do not vary. As the number of known SPsdBVs has increased, it has become clear that this group of pulsators is divided between the objects in the hot high-gravity part of the instability strip, which shows periods typically between 80 and 200 s, and the cooler low-gravity part where the objects have periods in the range 340−380 s.

The long-period pulsators were discovered very recently (Green et al. 2003). Stars in this class have lower temperatures (20 000−28 000 K) than the short-period pulsators, and the timescale of the long-period pulsations is typically more than an hour. These stars are now recognised to be *g*-mode pulsators, driven by the same iron opacity mechanism as the faster *p*-mode pulsators (Fontaine et al. 2004). The amplitude of the *g*-mode pulsations are very low, typically only about one millimagnitude, and a much larger fraction of sdB stars in the relevant temperature range displays this kind of pulsations than is the case for the *p*-mode pulsators.

Interestingly, two members of the class of SPsdBVs with pulsations in the range 340−380 s have now been found to also show *g*-mode pulsations: HS 0702+6043 (Schuh et al. 2005, 2006) and Balloon 090100001 (Oreiro et al. 2005; Baran et al. 2005).

The pulsating sdB star Balloon 090100001 (hereinafter BA09) got its designation as one of the FUV-bright high galactic latitude objects detected with a 13 cm balloon-bourne survey telescope. This telescope, the SCAP 2000, obtained photographic images in a bandpass of about 100 Å *FWHM* centered at about 2000 Å, and missions were flown between 1979 and 1990 (see e.g. Laget 1980). The significance of the Balloon designations is as follows: the first two digits identify the flight number, the next four digits refer to the plates on which the object is seen, and the last three digits give a running number.

Bixler et al. (1991) obtained spectral classifications for about 100 of the FUV-excess objects in the Balloon catalog and classified them as either sdB, sdO, WD or composite systems with a hot subluminous member. For BA09 they estimated an effective temperature of 32 500 K, which prompted one of us (RØ) to include the star in a list of candidate pulsators, which eventaully led to its discovery as the brightest sdB pulsator by Oreiro et al. (2004). Due to its convenient brightness (B = 11.8), BA09 has been observed intensely using 1 m class telescopes, leading to the recent discovery of more than 50 detected pulsational frequencies (Baran et al. 2006). Amongst these are *p*- and *g*-mode frequencies, including a triplet close to the dominant frequency of 2.8075 mHz. Altogether, the brightness, the pulsational amplitude, and the rich but seemingly non-randomly distributed frequency spectrum, make this star an excellent target for asteroseismological studies.

So far, only few pulsating sdB stars have been studied using time-resolved low-resolution spectroscopy on intermediate-size telescopes, e.g. PB 8783 and KPD 1209+4401 (Jeffery & Pollacco 2000), PG 1605+072 (O'Toole et al. 2003), PG 1325+101 (Telting & Østensen 2004). Recent high-resolution FUSE time-series of three sdBV were presented by Kuassivi et al. (2005). All these studies have shown that (low-resolution) spectroscopy gives additional information (with respect to photometric studies) regarding the fundamental parameters of the stars, and gives essential velocity information that further characterises the pulsational behaviour of these stars.

For studies of the pulsational characteristics of the modes, it is necessary to know the radial-velocity amplitudes corresponding to the modes. Whereas photometric measurements are sensitive to pulsational temperature variations only, spectroscopic measurements will reveal essential information regarding the pulsational velocity field. Telting & Østensen (2004) have shown for the case of PG 1325+101 that the radial-velocity information can be used to constrain the pulsational degree of the mode responsible for the observed variability, and that the radial-velocity information gives insight in the pulsational displacement and gravity amplitude at the surface of the star. In particular for advanced methods of mode identification (e.g. Daszynska-Daszkiewicz et al. 2005), the combination of photometric amplitude ratios and radial-velocity amplitudes discriminates the possible modes much more than photometric amplitude ratios alone.

In a recent asteroseismological application of Feige 48 based on period matching alone, the authors (Charpinet et al. 2005) argue that independent mode identifications, as may be achieved from time-series of multi-band photometry and/or spectroscopy, is needed to confirm their work.

In this paper we present the first results from time-resolved spectroscopy of BA09, based on our data set that was obtained with the aim to put constraints on the pulsational characteristics of this star. We focus on the frequency content of our data set, and derive radial velocities. The combination of these will be indispensable information for future mode-identification studies, and hence for detailed asteroseismological studies of Balloon 090100001. Further detailed modeling of the spectra, in terms of effective temperature, gravity, and the variations in those, will be presented in a separate paper.

2. Observations and reduction

On 7 nights in August/September 2004 we obtained in total more than 2500 time-resolved low-resolution spectra of Balloon 090100001 with the Nordic Optical Telescope using ALFOSC in long-slit spectroscopic mode (see Table 1). Our data set spans in total 38 nights, and overlaps with the photometric data set presented by Baran et al. (2006).

Our instrumental setup was: grism #16, CCD #8, and a long slit of 0.″8 width. This setup samples the wavelength region of approximately 3500−5050 Å, and gives a *FWHM* spectral resolution of about 3 Å, and a dispersion of 0.77 Å/pixel corresponding to 54 km s^{-1}/pixel at the center of the wavelength range. We set up the grism and slit such that the dispersion was along the rows of the CCD, which enabled a much shorter read-out time of the CCD with respect to the standard instrument setup. We used an exposure time of 30 s. With appropriate

Table 1. Log of spectra used for the frequency analysis. Dates are for start of night. HJD is given in seconds with respect to 2 453 241.0.

Date 2004	Heliocentric JD [s]	Number of spectra
23 Aug.	35 341–65 851	311
05 Sep.	1 182 363–1 186 260	90
08 Sep.	1 418 964–1 448 838	525
09 Sep.	1 502 031–1 535 133	621
13 Sep.	1 844 739–1 880 706	544
17 Sep.	2 208 796–2 219 860	221
29 Sep.	3 245 737–3 257 008	240

binning (×2) and windowing (1.6 arcmin), both in the spacial direction only, we achieved a cycle time of 43 s.

The object was acquired onto the slit and monitored until the slit angle rotated significantly away from the parallactic angle. A few re-acquisitions onto the slit were done during each night. Thorium-argon and helium arc-line spectra were made sandwiching 40 or less consecutive spectra. For each night typically 30 afternoon and morning flats were obtained with Halogen lamps for the purpose of removing CCD pixel-to-pixel variations.

The spectra were flatfielded and extracted using standard tasks within IRAF. Our flatfielding procedure did not suffice to remove some stable CCD structures in the bluest 250 Å of the spectra. We used the CCD overscan region to estimate the global bias level. Two bad columns were removed by linear interpolation of pixels in adjacent columns. One-dimensional spectra were optimally extracted after subtracting a fit to the sky background for each detector column. Wavelength calibration was done with the combined ThAr+He calibration spectra, interpolating the wavelength solution between the nearest before and after calibration spectra. The mean spectrum before normalisation is shown in Fig. 1.

The spectra were normalised first with respect to the mean spectrum, by fitting a cubic spline with between 6 to 10 segments to the quotient of each individual spectrum and the mean spectrum. Subsequently, the mean spectrum was normalized to the continuum, using an iterative procedure discarding points lying 2σ below a fit of 15 cubic spline segments. The resulting fit was used to rectify the individual spectra.

The target spectra were clipped to the range of 3512−5032 Å for our spectral analysis. The peak signal to noise ratio of the reduced spectra was typically around 50. All acquisition times and velocities were transformed to the heliocentric frame by correcting for the earth orbit and earth rotation only. We obtained in total 2552 useful spectra.

The 30 s exposure time of the spectra gives rise to phase smearing that reduces the amplitude of the pulsational radial-velocity variations, and any other type of variations derived from the spectra. Assuming a sinusoidal variation with the known main pulsation period of 356 s the smearing reduces the amplitude by only 1.2%, but the amplitude of a sine with the first harmonic of this period is reduced by 4.7%.

We find no obvious long-term radial-velocity variations exceeding the large instrumental trends. There are no obvious indications that the mean spectrum is of composite nature, which implies that Balloon 090100001 may not be part of a binary system. Note that the sharp Ca II K line does not move along with the pulsational velocity shifts, indicating that this line is of interstellar origin.

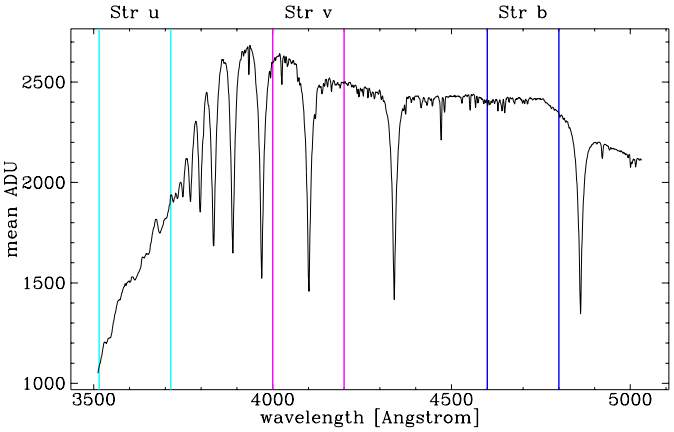

Fig. 1. Average of all 2552 unnormalised spectra, with domains used for *uvb* spectrophotometry.

We used H8–Hβ, He I 4026 Å, and He I 4471 Å in the mean of all 2552 spectra to estimate the average radial velocity of the star. We fitted Lorentzian and Gaussian profiles to the hydrogen and helium lines respectively, leading to $\langle v_{\rm rad}\rangle = -34 \pm 2\,{\rm km\,s^{-1}}$. From the interstellar Ca II 3933.664 Å line in the nightly averages we obtained a radial-velocity zero point of $5 \pm 4\,{\rm km\,s^{-1}}$. Combining these results we find for the radial space velocity of Balloon 090100001 $\langle v_{\rm rad}\rangle = -39 \pm 5\,{\rm km\,s^{-1}}$.

3. Fourier analyses

We calculated the radial velocity of the time-resolved spectra using the standard cross-correlation application in IRAF. The mean of all 2552 spectra served as the template spectrum. The center of the cross-correlation function (CCF) was fit in 25 velocity bins around the maximum with a Gaussian; the 25 bins approximately spanning the points within the *FWHM* of the CCF. The obtained radial-velocity shifts are dominated by those of the strongest Balmer lines in the spectrum. The results for one night are shown in Fig. 2: the vertical width of the radial-velocity curve reflects the pulsational variation of the main mode in Balloon 090100001. The radial velocities of the spectra are listed in Table 8 (available at CDS).

To analyse in detail the pulsational information that our dataset contains, we also used the *FWHM* of the CCF, which is a measure of the width of the Balmer lines, and hence a measure of surface gravity. Furthermore, we used the average equivalent width (*EW*) of the Hγ–H9 Balmer lines as a further observable. To beat the noise in the wings of the profiles, each point in the profile was weighted with its own depth with respect to the continuum, implying the following non-standard form $EW = \sqrt{\Sigma(1-P(\lambda))^2} \times \Delta\lambda$. See Fig. 2 for the *EW* of one night of data: again the vertical spread reflects the pulsational variation of the main mode.

We also used our unnormalised spectra to obtain quasi-Strömgren *uvb* photometry, from the mean count level in the following bands: 3515−3715 Å (roughly corresponding

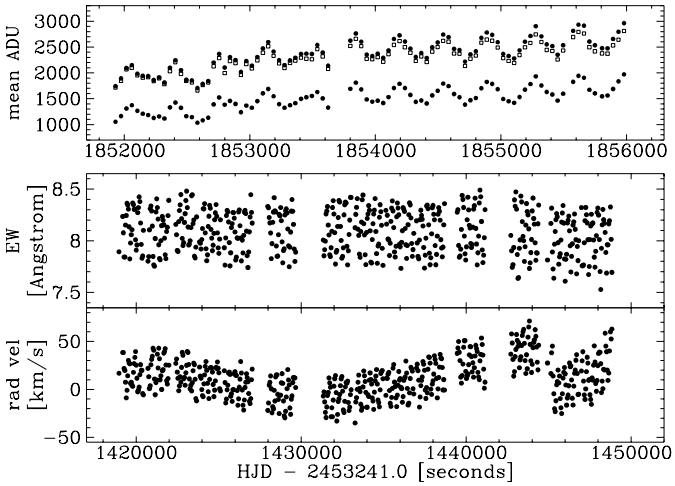

Fig. 2. *Top*: quasi-Strömgren *u* (lowest), *v* and *b* (squares) light curve for about 1 h of data. *Middle*: equivalent width variations of the Balmer lines for one night of data. *Bottom*: radial velocities for one night, obtained from cross-correlation of the time-resolved spectra.

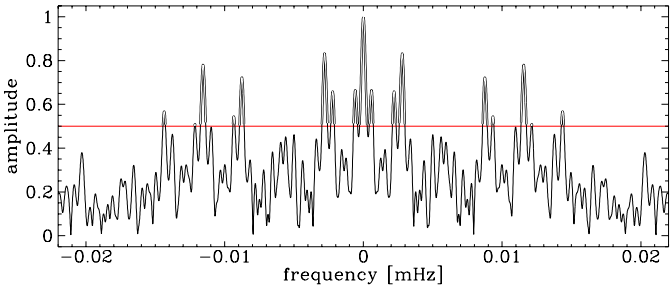

Fig. 3. Amplitude of the FT window funtion, showing clear 4-day and 1-day aliases.

Table 2. Amplitude of peaks in Fourier transform of the window function. The amplitude of the central window peak is normalized to 1.0. See Fig. 3.

Freq. [mHz]	Amplitude	ID
0.00059	0.664062	
0.00221	0.658503	
0.00280	0.831530	w_1
0.00876	0.722355	w_3
0.00934	0.544270	
0.01156	0.780013	w_2
0.01214	0.509230	
0.01436	0.566897	

to the redder half of a standard Strömgren *u* band pass), 4000−4200 Å, and 4600−4800 Å. For each band the mean count levels were put on a magnitude scale, to simulate photometric observations. Figure 1 shows the mean of 2552 extracted spectra, with the photometric bands indicated.

From Fig. 2 it is clear that from one telescope pointing to the next jumps in the radial-velocity curve are present, due to the repositioning of the object in the slit (see also Telting & Østensen 2004). Also between subsequent repointings, there are general trends in the data, which are largely due to instrumental effects. These instrumental velocity changes appear on timescales much longer than the main pulsation period of the star, but they do overlap the period range of the *g*-mode pulsations in this star.

In order to investigate the main pulsation mode and the other high-frequency modes in Balloon 090100001, we decided to detrend the observations by fitting a straight line or parabola to appropriate chunks of radial-velocity, *FWHM* and *uvb* data, where the chunks for the 3 photometry bands all had equal timings.

It was noted (see Fig. 2) that the *EW* curve was relatively clean with respect to long-term instrumental trends, and consequently we decided not to detrend these data in order to search for periodicities in the *g*-mode frequency domain.

3.1. Results from prewhitening

In Fig. 3 we show the Fourier transform (DFT) of the window function (expressed in amplitude rather than power). The distribution in time of the spectra results in strong 1-day and 4-day aliases. Although the frequency resolution as obtained from the central window peak is on the order of 0.6 μHz (*FWHM*), the severe aliasing pattern makes it difficult to separate real peaks from aliases. To compute the Fourier transforms we used a frequency step of 0.01 μHz, and a frequency range of [0−15 mHz].

Fortunately, there were two photometric campaigns of Balloon 090100001 (Oreiro et al. 2005; Baran et al. 2005) in the same observing period as ours. Baran et al. (2006) have combined these two photometric datasets and listed the resulting photometric frequencies of Balloon 090100001. Given the difficulties arising from aliasing in our spectroscopic dataset, we will below use the photometric frequencies to qualify the peaks found in our Fourier spectra.

We first analysed our data in terms of prewhitening sequences, for which the significance of a peak is judged by the 4 S/N criterion. Here the noise was estimated by the average amplitude in the Fourier spectrum in the frequency range [0−5 mHz], which was calculated after each individual prewhitening step. Tables 3 to 6 list the frequencies that survive the 4 S/N criterion, for the different observables. In the rightmost column identifications matching the frequencies in Baran et al. (2006) are listed.

Note that to match our frequencies with those of Baran et al. (2006), we considered all their listed frequencies convolved with our window function. For this convolution we used all frequencies for which the window function (see Fig. 3) has an amplitude of 0.5 or higher, in order to match only likely aliases. Although there are 8 alias peaks in our window function that fulfil this criterion, we found only aliases at the 3 strongest window peaks (see Table 3) and we found that all matched frequencies match within 0.1 μHz (except for one listed in Table 5).

The Fourier transforms of the *EW*, detrended *u* spectrophotometry and the detrended radial-velocity data are shown in Figs. 4 and 5; the latter figure shows the Fourier spectra after the first prewhitening step. It is clear from these figures and from Tables 3 to 6 that the main pulsation mode, corresponding to $f_1 = 2.8075$ mHz, dominates the variability in Balloon 090100001.

Table 3. Fourier results of prewhitening sequences for the detrended *uvb* spectrophotometry. Amplitude errors are estimated from the average amplitude in the interval [0–5 mHz], after each prewhitening cycle. Phases are given with respect to t = 1 607 216.7 s after t_0 = HJD 2 453 241.0. All listed ID's match Baran et al. (2006) within 0.1 μHz.

Freq. [mHz]	Amplitude [mmag]	Phase [radians]	ID
u spectrophotometry			
2.80750	76.2 ± 4.0	4.46	2.8075
2.83199	24.9 ± 3.6	3.02	2.8232 $+w_3$
(2.83383	15.2 ± 3.5	1.35	2.8250 $+w_3$)
1.08045	14.7 ± 3.5	1.82	
0.43011	13.9 ± 3.5	2.14	
v spectrophotometry			
2.80750	53.7 ± 3.7	4.47	2.8075
2.83199	20.1 ± 3.5	3.03	2.8232 $+w_3$
1.08046	14.9 ± 3.4	1.84	
0.43011	14.0 ± 3.4	2.15	
b spectrophotometry			
2.80750	49.9 ± 3.7	4.47	2.8075
2.83199	19.4 ± 3.4	3.04	2.8232 $+w_3$
1.08046	14.9 ± 3.4	1.84	
0.43010	14.0 ± 3.4	2.15	

Table 4. As Table 3 but for the detrended *FWHM* of the CCF. Phases are given with respect to t = 1 602 104.3 s after t_0 = HJD 2 453 241.0.

Freq. [mHz]	Amplitude [km s^{-1}]	Phase [radians]	ID
2.80749	12.2 ± 0.55	3.41	2.8075
2.82314	2.8 ± 0.46	4.93	2.8232
5.61498	2.5 ± 0.45	0.21	5.6149
0.03462	2.4 ± 0.45	6.09	
0.05522	2.1 ± 0.45	2.16	
2.82201	2.0 ± 0.44	0.98	2.8248 $-w_1$

It is also clear from the tables that the second frequency in Balloon 090100001, f_2 = 2.8232 mHz, is found at an alias in all our observables but the *FWHM* of the CCF. This means that the affected prewhitening sequences suffer from incorrect cleaning of the Fourier spectra from prewhitening step 2 onwards. To investigate the importance of this, we recalculated our prewhitening sequences forcing the first and second prewhitening frequencies to be f_1 and f_2. For our *uvb* bands the only difference in the results is that the detrended-*u*-band frequency 2.8338 mHz (indicated inbetween parentheses in Table 3) does not appear in the recalculated frequency list. For the detrended radial velocities and for the *EW*, the recalculated prewhitening sequences are listed in Tables 5 and 6 respectively. It is clear from these recalculated sequences that especially the triplet frequencies f_2, f_3 = 2.8248 mHz, and f_4 = 2.8264 mHz, suffer from aliasing problems, and that most other frequencies remain undisturbed by these effects. The frequency 2.8309 mHz seems a spurious result from the initial incorrect prewhitening sequence.

Table 5. As Table 4 but for the detrended radial velocities. The bottom part lists the prewhitening sequence for which the second prewhitening frequency is forced to 2.8232 mHz. All listed ID's match Baran et al. (2006) within 0.1 μHz, except for the one marked with a *.

Freq. [mHz]	Amplitude [km s^{-1}]	Phase [radians]	ID
2.80750	18.0 ± 0.52	4.94	2.8075
2.83196	4.9 ± 0.35	4.44	2.8232 $+w_3$
2.83094	2.6 ± 0.33	0.76	
2.81756	2.0 ± 0.32	3.14	2.8264 $-w_3$
0.32815	1.7 ± 0.31	5.33	
0.18104	1.7 ± 0.31	2.74	
0.29424	1.5 ± 0.30	4.12	
5.62784	1.4 ± 0.30	1.96	5.6307 $-w_1$
2.84621	1.3 ± 0.30	4.05	
0.46406	1.3 ± 0.29	2.90	
3.77610	1.2 ± 0.29	5.24	3.7761
2.80750	18.0 ± 0.52	4.94	2.8075
2.82318	4.7 ± 0.35	0.14	2.8232
2.82480	2.9 ± 0.33	4.47	2.8248
2.83804	1.8 ± 0.32	3.14	2.8264 $+w_2$
0.32815	1.8 ± 0.31	5.33	
0.18105	1.7 ± 0.31	2.74	
0.29425	1.5 ± 0.30	4.12	
2.81459	1.5 ± 0.30	4.05	2.8232 $-w_3$ *
5.62784	1.4 ± 0.30	1.96	5.6307 $-w_1$
0.46406	1.3 ± 0.30	2.90	
3.77610	1.2 ± 0.29	5.24	3.7761
2.76029	1.2 ± 0.29	4.05	

3.2. Previously known and possible new frequencies

From Tables 3 to 6 it is evident that we can confirm the following frequencies that were listed by Baran et al. (2006): f_1, f_2, f_3, f_4, $2f_1$, f_1+f_2, 3.7761 mHz, and the g-mode frequencies 0.2724 mHz, 0.3257 mHz, and 0.3658 mHz.

There are two other frequencies that are present in all our detrended-*uvb* band Fourier spectra: 0.4301 mHz and 1.0804 mHz. These have the same amplitudes in all 3 bands, which does not favour but which also does not exclude a pulsational origin. We stress that the detrending for all three bands has been done in an identical way, and that there are no obvious counterparts of these frequencies in the Fourier spectra of the undetrended *uvb* data.

We checked if the unmatched frequencies in Tables 3 to 6 are related to pulsational beat frequencies, or whether they could be eachother aliases (for the 3 main aliases). We note that 0.02464 mHz (*EW*) is close to an alias of f_1-f_2, and that 0.18105 mHz (radial velocity) and 0.19863 mHz (*EW*) could both be an alias of 0.18984 mHz.

In order to perform a consistency check for the unmatched frequencies of the *EW* Fourier spectra that are based on the average *EW* of the 6 strongest Balmer lines in our spectra, we also computed the average of the *EW* of two groups of 3 Balmer lines: with the first group H8, Hδ, and Hβ, and with the second group H9, Hϵ, and Hγ. If the frequencies that we find are of stellar origin, one would expect that all frequencies listed in Table 6 would show up in the Fourier spectra of both sets of 3-line *EW* data. The results of this excercise can be found

Table 6. As Table 4 but for the average *EW* of the Balmer lines. The bottom part lists the prewhitening sequence for which the second prewhitening frequency is forced to 2.8232 mHz. All listed ID's match Baran et al. (2006) within 0.1 μHz.

Freq. [mHz]	Amplitude [Å]	Phase [radians]	ID
2.80749	0.272 ± 0.0075	0.43	2.8075
0.00547	0.104 ± 0.0044	0.02	
(0.00360	0.080 ± 0.0040	0.68	)
2.83198	0.056 ± 0.0037	6.19	2.8232 $+w_3$
(2.83092	0.028 ± 0.0034	2.32	)
(0.02464	0.025 ± 0.0033	3.08	)
5.61496	0.023 ± 0.0033	4.31	5.6149
2.81475	0.023 ± 0.0033	2.97	2.8264 $-w_2$
0.00111	0.022 ± 0.0032	1.11	
3.77610	0.020 ± 0.0032	0.60	3.7761
0.36585	0.018 ± 0.0031	3.54	0.3658
0.27520	0.016 ± 0.0031	3.57	0.2724 $+w_1$
(0.10641	0.014 ± 0.0030	4.33	)
(0.03795	0.013 ± 0.0030	3.02	)
(2.81129	0.013 ± 0.0029	2.33	)
0.33721	0.013 ± 0.0029	1.70	0.3257 $+w_2$
(0.19863	0.012 ± 0.0029	1.79	)
5.62790	0.012 ± 0.0029	3.74	5.6307 $-w_1$
2.80749	0.272 ± 0.0075	0.43	2.8075
2.82320	0.055 ± 0.0044	1.79	2.8232
(0.00547	0.104 ± 0.0042	0.02	)
(0.00359	0.080 ± 0.0037	0.69	)
2.82642	0.032 ± 0.0034	2.23	2.8264
(0.02464	0.026 ± 0.0033	3.10	)
5.61496	0.023 ± 0.0033	4.32	5.6149
(0.00111	0.022 ± 0.0033	1.12	)
3.77610	0.020 ± 0.0032	0.62	3.7761
2.83646	0.020 ± 0.0031	5.91	2.8248/2.8250 $+w_2$
0.36585	0.018 ± 0.0031	3.53	0.3658
0.27521	0.015 ± 0.0030	3.58	0.2724 $+w_1$
(0.10640	0.014 ± 0.0030	4.35	)
(2.85946	0.014 ± 0.0030	4.12	)
(0.03795	0.013 ± 0.0029	3.03	)
0.33723	0.013 ± 0.0029	1.69	0.3257 $+w_2$
(0.19863	0.013 ± 0.0029	1.79	)
2.81083	0.012 ± 0.0028	3.31	
5.62791	0.012 ± 0.0028	3.75	5.6307 $-w_1$

in Table 6, where we put all unmatched frequencies that do not show up consistently and significantly in the Fourier analyses of both groups of 3-line *EW* data inbetween parentheses. As one can see, almost none of the unmatched low-frequency *EW* peaks survive this consistency check, and we conclude that they are probably due to long-term observational/instrumental trends.

There are a few low-frequency peaks in our Fourier spectrum of the detrended radial velocities (Table 5) that fall in the frequency range of the possible g-modes listed by Baran et al. (2006), but none of our frequencies matches those of Baran et al. We note however that our frequency 0.32815 mHz is close to an alias of their frequency 0.3257 mHz, and close to an alias of their frequency 0.3312 mHz.

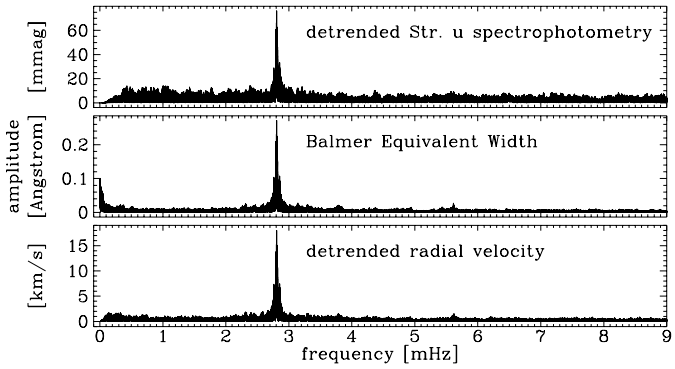

Fig. 4. Fourier transforms.

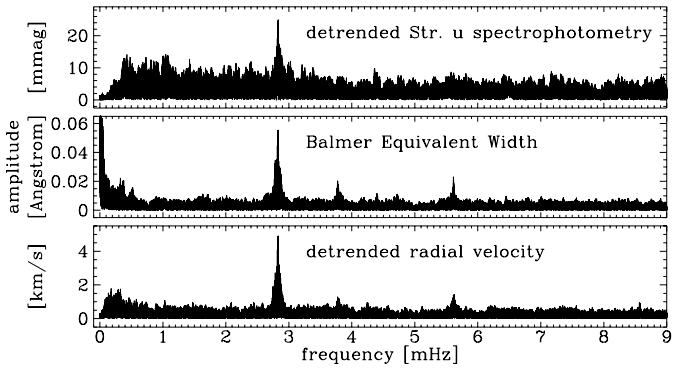

Fig. 5. As Fig. 4 after prewhitening with the main pulsation frequency 2.8075 mHz.

Our general conclusion is that we do not find conclusive evidence for stellar frequencies that were not already previously known. After scrutinizing our frequency tables a few significant frequencies remain, but these should not be considered as real frequencies unless they can be confirmed from other data sets of Balloon 090100001.

3.3. Radial-velocity amplitudes from sine fits

In studies of the pulsational characteristics of the modes, it is necessary to know the radial-velocity amplitudes corresponding to the modes. In particular for some methods of mode identification (e.g. Daszynska-Daszkiewicz et al. 2005), the combination of radial-velocity amplitudes and photometric amplitude ratios discriminates the possible modes much more than photometric amplitude ratios alone.

For this purpose we have fitted our radial-velocity data, using a model of multiple sinusoids. The frequencies included are that of the 10 secure frequencies listed in the previous subsection; two of these are combination frequencies.

We first fitted the model of 10 sinusoids and an offset to the detrended and undetrended radial velocities of the 2552 spectra, keeping the frequencies fixed to those found in the Fourier analysis (Sect. 3.1). We subsequently optimized the frequencies within their local χ^2 maxima. For the fits we assumed an error of 5 km s^{-1} on each radial-velocity measurement, which lead to a normalised $\chi^2 = 2.2$ for the detrended data set.

The results of the fits are listed in Table 7. It is clear from the fit results of the g-mode frequencies that the detrending

Table 7. Results of fits of model of 10 sinusoids to radial velocities. Phases are given in seconds with respect to HJD = 2 453 241.0, and amplitudes are in km s^{-1}.

Undetrended V_{rad}			Detrended V_{rad}		
Freq. [mHz]	Amplitude	Phase	Freq [mHz]	Amplitude	Phase
0.27255 (1)	2.70 (14)	1023 (75)	0.27244 (3)	0.86 (14)	80 (229)
0.32591 (1)	2.67 (15)	403 (74)	0.32567 (3)	0.96 (14)	1637 (175)
0.36567 (1)	2.69 (15)	1301 (57)	0.36577 (3)	1.05 (14)	–724 (138)
2.80748 (1)	19.17 (17)	68 (1)	2.80747 (1)	18.89 (16)	63 (1)
2.82324 (1)	6.20 (27)	104 (4)	2.82324 (1)	5.88 (23)	101 (4)
2.82484 (1)	3.56 (21)	63 (9)	2.82481 (2)	3.44 (21)	51 (11)
2.82625 (3)	1.90 (28)	41 (15)	2.82628 (3)	1.84 (28)	46 (20)
3.77610 (2)	1.38 (14)	–20 (10)	3.77610 (2)	1.27 (14)	–18 (11)
5.61502 (3)	1.10 (14)	–7 (9)	5.61503 (3)	1.27 (14)	–1 (8)
5.63065 (4)	0.86 (14)	–32 (12)	5.63065 (3)	0.99 (14)	–29 (11)

affects the data significantly, and that the amplitudes and phases should be taken with caution.

For the *p*-mode frequencies the results are consistent for the detrended and undetrended data sets. Note that the amplitude of $f_2 = 2.82324$ mHz is much larger than found in the Fourier analysis, which is explained by the aliasing problems discussed above (Sect. 3.1). The radial-velocity amplitude of the main pulsation mode ($f_1 = 2.80749$ mHz) in Balloon 090100001 is 18.9 km s^{-1}, as established from the fit to the detrended data set.

It remains to be investigated from extensive follow-up observations whether the observed amplitudes are stable from one observing season to the next. As is the case for PG 1605-072 (see O'Toole et al. 2000, 2002, 2005; Woolf et al. 2002; Falter et al. 2003), it is possible that also in Balloon 090100001 some of the observed amplitudes may change over time.

4. Conclusions

We obtained the first large time-resolved spectroscopic data set of Balloon 090100001, comprising 2552 low-resolution spectra. Our average spectrum with outstanding signal to noise ratio does not show any clear evidence of a possible companion, ruling out companions other than a possible white dwarf or dM star. The variability in the spectra is dominated by the main pulsation mode in Balloon 090100001.

We used the cross-correlation technique to derive radial velocities, with the mean spectrum as a template (see Table 8 which is published electronically). The radial-velocity amplitude of the main pulsation mode ($f_1 = 2.80749$ mHz) in Balloon 090100001 is 18.9 km s^{-1}, which is the largest pulsational radial-velocity amplitude observed in sdB stars.

We performed Fourier analyses of several observables measured from the spectra, and used the photometrically derived frequency spectrum of Baran et al. (2006, who presented a contemporary data set) to match our frequency list. We found 2 previously known frequencies in our quasi-Strömgren *uvb* bands, 4 previously known frequencies in the *FWHM* of the cross-correlation function, 7 previously known frequencies in the radial velocities, and as much as 10 previously known frequencies in the average weighted equivalent width (*EW*) of the Balmer lines. The 10 *EW* frequencies contain all the frequencies found in the other observables. Thus, we confirmed ten of the strongest frequencies found by Baran et al. (2006), among which are the dominant mode f_1, the triplet frequencies $f_2 - f_4$, and 4 other independent *p*-mode and *g*-mode frequencies. Out of these ten frequencies, eight are independent, which implies that future mode-identification studies of this star are constrained by combined photometric and spectroscopic observations for as much as 8 pulsation modes. After PG 1605+072 (O'Toole et al. 2005) this is only the second subdwarf for which such a rich pulsational spectrum has been detected in combined photometric and spectroscopic data.

We note that due to instrumental/observational effects we had to detrend all observables but the *EW*. This may be part of the reason why the 3 *g*-mode frequencies detected in the *EW* are not seen in other observables such as the radial velocity.

Although we found other statistically significant peaks, we suspect that many of them are spurious, as indicated by the consistency check discussed in Sect. 3.2. We therefore conclude that our dataset does not suffice to conclusively ascribe these additional frequencies to be intrinsic to the star: confirmation is needed from other data sets that are less affected by aliasing.

We have argued that Balloon 090100001, being the brightest pulsating sdB in the sky with the largest known pulsational radial-velocity amplitude, and which has a rich pulsational frequency spectrum, is an excellent target for asteroseismological studies that aim to improve our understanding of the internal

Table 8. Radial velocities (undetrended) in km s^{-1} of all 2552 spectra with respect to that of the mean spectrum, as obtained from cross-correlation. See the text for the radial velocity of the mean spectrum. HJD is given in seconds with respect to HJD = 2 453 241.0.

	HJD	Velocity
1	35 341.06	–14.4
2	35 424.00	–25.3
3	35 524.22	–24.5
.	.	.
.	.	.
.	.	.
2550	3 256 922.30	9.3
2551	3 256 964.64	0.8
2552	3 257 008.70	19.6

structure of subdwarf B stars. Our dataset forms an excellent starting point for further modelling of the pulsational characteristics of Balloon 090100001, which will be addressed in a separate paper (Østensen et al., in prep.: Paper II).

Acknowledgements. We especially thank Dr. Thomas Augusteijn for obtaining the last 240 spectra of our data set in service mode during technical time.
The data presented here have been taken using ALFOSC, which is owned by the Instituto de Astrofisica de Andalucia (IAA) and operated at the Nordic Optical Telescope under agreement between IAA and the NBIfAFG of the Astronomical Observatory of Copenhagen.
Based on observations made with the Nordic Optical Telescope, operated on the island of La Palma jointly by Denmark, Finland, Iceland, Norway, and Sweden, in the Spanish Observatorio del Roque de los Muchachos of the Instituto de Astrofisica de Canarias.

References

Baran, A., Pigulski, A., Kozieł, D., et al. 2005, MNRAS, 360, 737
Baran, A., Oreiro, R., Pigulski, A., et al. 2006, Baltic Astron., 15, 241 [preliminary page-number]
Bixler, J. V., Bowyer, S., & Laget, M. 1991, A&A, 250, 370
Charpinet, S., Fontaine, G., Brassard, P., & Dorman, B. 1996, ApJ, 471, L106
Charpinet, S., Fontaine, G., Brassard, P., et al. 1997, ApJ, 483, L123
Charpinet, S., Fontaine, G., Brassard, P., et al. 2005, A&A, 443, 251
Daszynska-Daszkiewicz, J., Dziembowski, W. A., & Pamyatnykh, A. A. 2005, A&A, 441, 641
Dorman, B., O'Connell, R. W., & Rood, R. T. 1993, ApJ, 419, 596
D'Cruz, N. L., Dorman, B., Rood, R. T., & O'Connell, R. W. 1996, ApJ, 466, 359
Falter, S., Heber, U., Dreizler, S., et al. 2003, A&A, 401, 289
Fontaine, G., Green, E. M., Brassard, P., et al. 2004, Ap&SS, 291, 379
Green, E. M., Fontaine, G., Reed, M. D., et al. 2003, ApJ, 583, L31
Han, Z., Podsiadlowski, P., Maxted, P. F. L., Marsh, T. R., & Ivanova, N. 2002, MNRAS, 336, 448
Han, Z., Podsiadlowski, P., Maxted, P. F. L., & Marsh, T. R. 2003, MNRAS, 341, 669
Heber, U. 1986, A&A, 155, 33
Jeffery, C. S., & Pollacco, D. 2000, MNRAS, 318, 974
Kilkenny, D., Koen, C., O'Donoghue, D., & Stobie, R. S. 1997, MNRAS, 285, 640
Kuassivi, Bonanno, A., & Ferlet, R. 2005, A&A, 442, 1015
Laget, M. 1980, A&A, 81, 37
Milliard, B., Donas, J., & Laget, M. 1991, Adv. Space Res., 11, 135
Oreiro, R., Ulla, A., Pérez Hernández, F., et al. 2004, A&A, 418, 243
Oreiro, R., Pérez Hernández, F., Ulla, A., et al. 2005, A&A, 438, 257
O'Toole, S. J., Bedding, T. R., Kjeldsen, H., et al. 2000, ApJ, 537, L53
O'Toole, S. J., Bedding, T. R., Kjeldsen, H., Dall, T. H., & Stello, D. 2002, MNRAS, 334, 471
O'Toole, S. J., Jørgensen, M. S., Kjeldsen, H., et al. 2003, MNRAS, 340, 856
O'Toole, S. J., Heber, U., Jeffery, C. S., Dreizler, S., et al. 2005, A&A, 440, 667
Saffer, R. A., Bergeron, P., Koester, D., & Liebert, J. 1994, ApJ, 432, 351
Schuh, S., Huber, J., Green, E., et al. 2005, in 14th Workshop on White Dwarfs, ed. D. Koester, & S. Moehler, ASP Conf. Ser., 334, 530
Schuh, S., Huber, J., Dreizler, S., et al. 2006, A&A, 445, L31
Telting, J. H., & Østensen, R. H. 2004, A&A, 419, 685
Woolf, V. M., Jeffery, C. S., & Pollacco, D. L. 2002, MNRAS, 329, 497